Uniform theoretical description of plasmon-induced transparency in plasmonic stub waveguide

Guangtao Cao,[1,2] Hongjian Li,[1,2,*] Shiping Zhan,[1] Zhihui He,[1] Zhibo Guo,[1] Xiuke Xu,[1] and Hui Yang[1]

[1]*College of Physics and Electronics, Central South University, Changsha 410083, China*

[2]*College of Materials Science and Engineering, Central South University, Changsha 410083, China*

**Corresponding author: lihj398@csu.edu.cn*

Received May 16, 2013; revised October 31, 2013; accepted December 1, 2013;
posted December 4, 2013 (Doc. ID 190570); published January 6, 2014

We investigate a classic analog of electromagnetically induced transparency (EIT) in a metal–dielectric–metal (MDM) bus waveguide coupled to two stub resonators. A uniform theoretical model, for both direct and indirect couplings between the two stubs, is established to study spectral features in the plasmonic stub waveguide, and the theoretical results agree well with the finite difference time domain simulations. Adjusting phase difference and coupling strength of the interaction, one can realize the EIT-like phenomena and achieve the required slow light effect. The theoretical results may provide a guideline for the control of light in highly integrated optical circuits.

OCIS codes: (240.6680) Surface plasmons; (230.7370) Waveguides; (130.3120) Integrated optics devices.
http://dx.doi.org/10.1364/OL.39.000216

Electromagnetically induced transparency (EIT) observed in atomic media is attributed to the quantum interference of pump and probe laser beams tuned at different transitions [1,2]. The demanding experimental conditions required to observe the EIT effect hinder its practical application, which catalyzes an ongoing search for classical systems mimicking EIT. The dielectric photonic resonator system is one of them [3–6]. It is noteworthy that controlling light on a small scale is very essential for highly integrated optics. Surface plasmon polaritons (SPPs) propagating along the metal–dielectric interface can be well confined by ultrasmall metal structures and break the diffraction limit [7,8]. Among different plasmonic devices, metal–dielectric–metal (MDM) plasmonic waveguides have attracted much attention, because they support modes with deep wavelength scale and an acceptable propagation length for SPPs. Based on the unique feature of MDM, the plasmonic analog of EIT observed in nanoscale plasmonic resonator systems was theoretically predicted and experimentally demonstrated in recent research [9–22]. Huang and co-workers, using the transmission line theory and scattering matrix theory, introduced the subwavelength slow-light mode in periodic-stub-assisted plasmonic waveguides [9,10]. In [14], Lu *et al.* demonstrated phase-coupled, plasmon-induced transparency [18] in plasmonic systems consisting of nanodisk resonators aperture-side-coupled to MDM bus waveguides. According to the coupling between bright and dark modes, Piao *et al.* demonstrated the control of spectral asymmetry in EIT-like spectral responses [16]. Haus and co-workers studied the EIT-like transmission by direct and indirect couplings between two stub resonators based on the temporal coupled mode theory (CMT) [19,20] and Fabry–Perot (FP) model, respectively [21]. In [22], Chen *et al.* experimentally and numerically showed the EIT-like transmission in terahertz asymmetric waveguide with two stubs. However, very few uniform analytical descriptions have been performed on plasmon-induced transparency in plasmonic stub waveguides for both direct and indirect couplings between the two stub resonators.

In this Letter, we investigate the EIT-like spectral responses in a plasmonic system composed of an MDM bus waveguide coupled to two stub resonators with either direct or indirect coupling. Although the system is similar to the schematic reported in [22], we present a uniform analytical description of plasmon-induced transparency for both direct and indirect couplings based on the CMT. To validate the correctness of the theoretical results, we have compared them with the FDTD simulations [23].

Figure 1 is a schematic illustration of an MDM waveguide coupled to two stub resonators. The insulator and metal in the structure are air and silver, respectively. The permittivity of silver is characterized by the Drude model $\varepsilon(\omega) = 1 - \omega_p^2 - (\omega^2 + i\omega\gamma_p)$, with $\omega_p = 1.38 \times 10^{16}$ rad/s and $\gamma_p = 2.73 \times 10^{13}$ rad/s. These parameters are obtained by fitting the experimental results [24]. The main structure parameters are the width of waveguide and stubs (w), length of the stub resonators (d_1 and d_2), and coupling distance between the two stubs (L). We perform the FDTD simulations with a perfect matched layer (PML) boundary condition. The grid size in the x and y directions are chosen to be 5 nm × 5 nm for good convergence of the numerical calculations. Two power monitors P and O are set to detect the incident power P_{in} and transmitted power P_{out} at the locations. The transmittance is defined to be $T = P_{\text{out}}/P_{\text{in}}$. When the TM polarization light is incident along the x axis, the SPP wave can be formed on the metal–insulator interfaces and confined in the waveguide.

Based on the phase difference and hybridization between resonant modes of the two stub resonators, the dynamic transmission characteristics of the proposed structure can be analyzed by the CMT. $S_{p,\text{in}}^{(N)}$ and $S_{p,\text{out}}^{(N)}$ $(N = 1, 2)$ stand for the incoming and outgoing waves in the bus waveguide, as shown in Fig. 1. The energy amplitude a_N of the Nth resonator can be expressed as

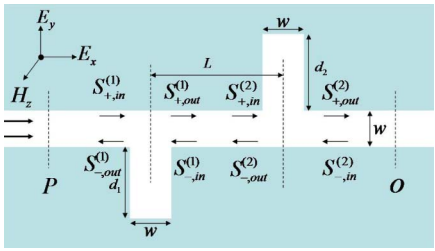

Fig. 1. Schematic of MDM waveguide coupled to two stub resonators.

$$\frac{da_1}{dt}=\left(-j\omega_1-\frac{1}{\tau_{i1}}-\frac{1}{\tau_{w1}}\right)a_1+S^{(1)}_{+,\mathrm{in}}\sqrt{\frac{1}{\tau_{w1}}}+S^{(1)}_{-,\mathrm{in}}\sqrt{\frac{1}{\tau_{w1}}}-j\mu_{12}a_2, \tag{1}$$

$$\frac{da_2}{dt}=\left(-j\omega_2-\frac{1}{\tau_{i2}}-\frac{1}{\tau_{w2}}\right)a_2+S^{(2)}_{+,\mathrm{in}}\sqrt{\frac{1}{\tau_{w2}}}+S^{(2)}_{-,\mathrm{in}}\sqrt{\frac{1}{\tau_{w2}}}-j\mu_{21}a_1, \tag{2}$$

where ω_N $(N=1,2)$ is the resonant frequency of the Nth stub resonator, $1/\tau_{iN}=\omega_N/(2Q_{iN})$ is the decay rate due to intrinsic loss in the Nth stub, $1/\tau_{wN}=\omega_N/(2Q_{wN})$ is the decay rate due to energy escaping into the bus waveguide, and $\mu_{12}=\omega_2/(2Q_c)$ and $\mu_{21}=\omega_1/(2Q_c)$ are the coupling coefficients between the two resonant modes. Q_{iN}, Q_{wN}, and Q_c are cavity quality factors related to intrinsic loss, waveguide coupling loss, and direct coupling between two stubs. With the conservation of energy, we get

$$S^{(1)}_{-,\mathrm{in}}=S^{(2)}_{-,\mathrm{out}}e^{j\varphi}, \tag{3}$$

$$S^{(2)}_{+,\mathrm{in}}=S^{(1)}_{+,\mathrm{out}}e^{j\varphi}, \tag{4}$$

$$S^{(1)}_{+,\mathrm{out}}=S^{(1)}_{+,\mathrm{in}}-\sqrt{\frac{1}{\tau_{w1}}}a_1, \tag{5}$$

$$S^{(2)}_{-,out}=S^{(2)}_{-,\mathrm{in}}-\sqrt{\frac{1}{\tau_{w2}}}a_2, \tag{6}$$

$$S^{(2)}_{+,\mathrm{out}}=S^{(2)}_{+,\mathrm{in}}-\sqrt{\frac{1}{\tau_{w2}}}a_2, \tag{7}$$

where the phase difference $\varphi=\mathrm{Re}(\beta_{\mathrm{SPP}})L=\omega\,\mathrm{Re}(n_{\mathrm{eff}})L/c$, with L being the coupling distance between the two stubs and c being the light velocity in vacuum. β_{SPP} and n_{eff} are propagation constant and effective index for SPPs [25,26], respectively.

Using boundary conditions of $S^{(2)}_{-,\mathrm{in}}=0$ and Eqs. (3)–(7), we finally arrive at the transfer function of the system,

$$t=\frac{S^{(2)}_{+,\mathrm{out}}}{S^{(1)}_{+,\mathrm{in}}}=e^{j\varphi}+\left(\gamma_1\frac{1}{\tau_{w2}}+\gamma_2\frac{1}{\tau_{w1}}+\chi_2\sqrt{\frac{1}{\tau_{w1}\tau_{w2}}}e^{j\varphi}+\chi_1\sqrt{\frac{1}{\tau_{w1}\tau_{w2}}}e^{-j\varphi}\right)(\gamma_1\gamma_2-\chi_1\chi_2)^{-1}e^{j\varphi}, \tag{8}$$

where $\gamma_1=(j\omega-j\omega_1-1/\tau_{i1}-1/\tau_{w1})$, $\gamma_2=(j\omega-j\omega_2-1/\tau_{i2}-1/\tau_{w2})$, $\chi_1=e^{j\varphi}(\tau_{w1}\tau_{w2})^{-1/2}+j\mu_{21}$, and $\chi_2=e^{j\varphi}(\tau_{w1}\tau_{w2})^{-1/2}+j\mu_{12}$. The transmittance efficiency can be derived as $T=|t|^2$. Figure 2(a) shows the transmittance spectra obtained from the same constructive parameters ($w=100$ nm, $d_1=300$ nm, $d_2=290$ nm), yet with different coupling distance $L=150$, 100, 50, and 0 nm. The circles and solid lines are calculated by the FDTD method and the CMT, respectively, and the theoretical results are in good agreement with FDTD simulations. For theoretical transmission spectra, $\omega_1=3.263\times10^{15}$ rad/s, $\omega_2=3.429\times10^{15}$ rad/s, $1/\tau_{w1}=10\times10^{12}$ rad/s, $1/\tau_{w2}=11\times10^{12}$ rad/s, $1/\tau_{i1}=3.45\times10^{12}$ rad/s, $1/\tau_{i2}=3.81\times10^{12}$ rad/s, and $\mathrm{Re}(n_{\mathrm{eff}})=1.25$. The coupling coefficients $\mu_{21}(\mu_{12})$ corresponding to $L=150$, 100, 50, and 0 nm are 2.3×10^{13} rad/s, 5×10^{13} rad/s, 9×10^{13} rad/s, and 16×10^{13} rad/s (2.417×10^{13} rad/s, 5.254×10^{13} rad/s, 9.458×10^{13} rad/s, and 16.814×10^{13} rad/s), respectively. It is found that the transparent peak presents a shift and the transparent window exhibits widening with the decrease of L, introducing the variation of the phase difference and coupling strength.

For Fig. 2(a), the coupling coefficient μ_{21} and coupling quality factor Q_c versus coupling distance L are plotted

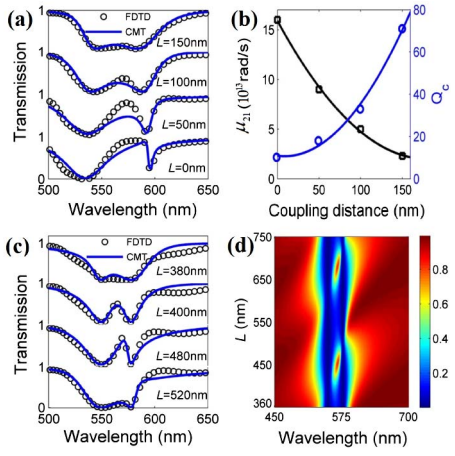

Fig. 2. (a) and (c) Transmission spectra with different coupling distance L between the two stub resonators. (b) Coupling coefficient and coupling quality factor versus coupling distance L. (d) Evolution of the transmission spectra versus L and λ. The other geometrical parameters are $w=100$ nm, $d_1=300$ nm, and $d_2=290$ nm. The circles are the simulation results and the solid curves are the analytical fits using the CMT.

in Fig. 2(b). We find that there is a trade-off between coupling coefficient μ_{21} and coupling quality factor Q_c. Coupling coefficient μ_{21} (coupling quality factor Q_c) decreases (increases) and the slope of $\mu_{21}(Q_c)$ gets smaller and smaller (larger and larger) with the increase of coupling distance L. The EIT-like optical response results from the destructive interference of electromagnetic fields from the two resonators, which is similar to what happens in metamaterial-induced transparency. Is the theoretical description (CMT) also suitable for the case in which the two stub resonators can only interact with each other indirectly? In this case, the quality factor $Q_c \to \infty$ and Eq. (8) can be expressed in the following form:

$$t = e^{j\varphi} + e^{j\varphi}\frac{\gamma_1\frac{1}{\tau_{w2}} + \gamma_2\frac{1}{\tau_{w1}} + 2\chi\sqrt{\frac{1}{\tau_{w1}\tau_{w2}}}\cos\varphi}{\gamma_1\gamma_2 - \chi^2}, \quad (9)$$

with $\chi = \chi_1 = \chi_2 = e^{j\varphi}(\tau_{w1}\tau_{w2})^{-1/2}$ and the other parameters being identical to those of Fig. 2(a).

Based on Eq. (9) and the FDTD method, we show the transmission spectra with coupling distance L in Fig. 2(c). It is apparent that the indirect coupling case is consistent with phase-coupled plasmon-induced transparency [14,21]. In Figs. 2(a) and 2(c), theoretical results are in good accordance with the FDTD simulations, from which we can conclude that Eq. (8) is a uniform theoretical description of plasmon-induced transparency in the plasmonic stub waveguide. So, the theoretical analysis allows us to understand the response of the plasmonic resonator system as a function of their microscopic parameters. To investigate spectral characteristics more specifically, the evolution of transmission spectra with the coupling distance L is shown in Fig. 2(d). As expected, the transparent band is between the two individual stub resonator resonances. Moreover, the transparent resonance peak exhibits a shift and its symmetry is tunable, which is in accordance with [14,21].

Slow light is one of the most important applications for EIT effect in atom systems, and the plasmonic system also supports slow group velocities [27,28]. Group index (n_g) in the plasmonic waveguide system can be calculated according to the following formula [14,29,30]:

$$n_g = \frac{c}{v_g} = \frac{c}{l}\tau_g = \frac{c}{l}\frac{d\theta}{d\omega}, \quad (10)$$

where c is the speed of light in vacuum, τ_g is the optical delay time, θ is the transmission phase shift, v_g stands for the group velocity, and l is the length of the plasmonic system.

In Figs. 3(a)–3(d), we plot the group index as the coupling distance L varies from 150 to 0 nm in steps of 50 nm. The other geometrical parameters are $w = 100$ nm, $d_1 = 300$ nm, and $d_2 = 290$ nm. For $L = 150$ nm and 100 nm, the typical features of plasmon-induced transparency are presented. The normal dispersion, which leads to a significantly enhanced group delay, occurs in the transparent window, but the abnormal dispersion (not discussed here) occurs around the plasmonic resonance

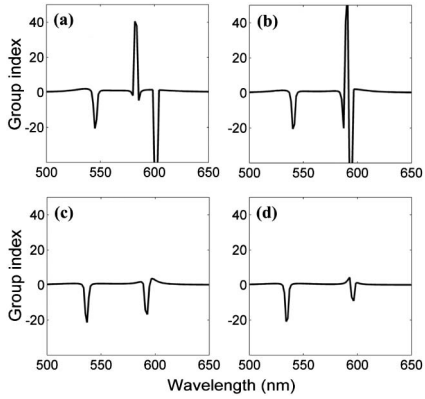

Fig. 3. Group index in the plasmonic stub waveguide for coupling distance (a) $L = 150$ nm, (b) $L = 100$ nm, (c) $L = 50$ nm, and (d) $L = 0$ nm. The other geometrical parameters are $w = 100$ nm, $d_1 = 300$ nm, and $d_2 = 290$ nm.

frequency. For $L = 50$ nm and 0 nm, normal dispersion in the transparent window nearly disappears. From Eqs. (8) and (10), we can obtain that the slow light effect, in the plasmonic system shown in Fig. (1) ($w = 100$ nm, $d_1 = 300$ nm, and $d_2 = 290$ nm.), is not obvious in the transparent window when coupling distance L is in the range of 0–90 nm, while an obvious slow effect can be observed for L larger than 90 nm, which may provide a guideline for the development of ultracompact optical buffers. What impact do the phase difference and coupling strength, respectively, have on plasmon-induced transparency?

In order to analyze the effects of phase difference and coupling strength on EIT-like transmission, the two stubs with changing coupling strength are set to be identical. In this case, Eq. (8) can be expressed as

$$t = e^{j\varphi} + e^{j\varphi}\frac{1}{\tau_w}\frac{2\gamma + 2\chi\cos\varphi}{\gamma^2 - \chi^2}, \quad (11)$$

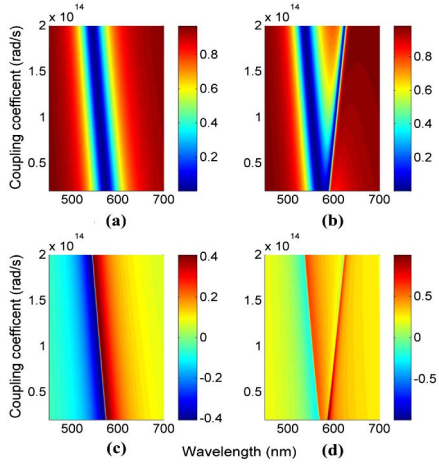

Fig. 4. Evolution of transmission spectrum with coupling coefficient μ for coupling distance (a) $L = 0$ nm and (b) $L = 50$ nm. (c) and (d) are transmission phase shifts corresponding to (a) and (b), respectively. The other geometrical parameters are $w = 100$ nm and $d_1 = d_2 = 300$ nm.

where $\omega_0 = \omega_1 = \omega_2$, $1/\tau_w = 1/\tau_{w1} = 1/\tau_{w2}$, $1/\tau_i = 1/\tau_{i1} = 1/\tau_{i2}$, $\mu = \mu_{12} = \mu_{21}$, $\gamma = \gamma_1 = \gamma_2 = j\omega - j\omega_0 - 1/\tau_i - 1/\tau_w$, and $\chi = \chi_1 = \chi_2 = e^{j\varphi}/\tau_w + j\mu$.

From Eq. (11), we show the transmission spectra versus coupling coefficient μ in Figs. 4(a) and 4(b), corresponding to $L = 0$ and 50 nm, respectively. The other parameters of the system are set as follows: $w = 100$ nm, $d_1 = d_2 = 300$ nm. Figure 4(a) shows that there is only one transmission dip which presents blue shift with the increase of coupling coefficient for $L = 0$ nm. In Fig. 4(b), the width of the transparent window becomes larger with the increase of coupling coefficient; however, transmission peak center remains nearly unmoved. Comparing Fig. 4(a) with 4(b), we can conclude that phase difference φ gives rise to EIT-like phenomena in the two-identical-stub system, that is to say, phase difference φ plays an important role in this transmission response. Combining Figs. 2(d) and 4(b), we can see that the shift of transmission peak center is caused by the phase difference, and the variation of transparent bandwidth is attributed to the coupling strength, which may pave a way toward dynamic control of plasmon-induced transparency by direct and indirect couplings in plasmonic stub waveguide. In Eq. (10), it is definite that group index is proportional to the dispersion velocity of transmission phase shift. Figures 4(c) and 4(d) depict the transmission phase shift ($\theta = \arg(t)$) corresponding to Figs. 4(a) and 4(b), respectively. In Figs. 4(c) and 4(d), there is a sudden phase jump around the transmission dip, but the normal dispersion in the transparent window is not obvious. Therefore, one could change phase difference and coupling strength of the interaction between the two stubs to realize EIT-like phenomena, and hence achieve the required slow light effect.

In summary, by using the temporal CMT and FDTD method, we have demonstrated the plasmonic analog of EIT in a plasmonic stub waveguide. The consistency between the theoretical and numerical results validates the correctness of the uniform theoretical description. For the direct coupling, there is a trade-off between coupling coefficient μ_{21} and coupling quality factor Q_c. In addition, the theoretical analysis shows that the EIT-like spectral response and slow light effect can be tuned easily by adjusting the coupling distance L. For both the direct and indirect couplings, phase difference and coupling strength between the two stub resonators contribute to the shift of transmission peak center and the variation of transparent bandwidth, respectively. The results may open up avenues for designing nanoscale optical switching, ultrasensitive sensors, and slow light devices in highly integrated optical circuits.

This work was funded by the Fundamental Research Funds for the Central Universities of Central South University under Grant Nos. 2012zzts007 and 2013zzts009, the Research Fund for the Doctoral Program of Higher Education of China under Grant No. 20100162110068, and the National Natural Science Foundation of China under Grant No. 61275174.

References

1. K. J. Boller, A. Imamolu, and S. E. Harris, Phys. Rev. Lett. **66**, 2593 (1991).
2. M. Fleischhauer, A. Imamoglu, and J. P. Marangos, Rev. Mod. Phys. **77**, 633 (2005).
3. Q. Xu, S. Sandhu, M. L. Povinelli, J. Shakya, S. Fan, and M. Lipson, Phys. Rev. Lett. **96**, 123901 (2006).
4. X. Yang, M. Yu, D. L. Kwong, and C. W. Wong, Phys. Rev. Lett. **102**, 173902 (2009).
5. K. Totsuka, N. Kobayashi, and M. Tomita, Phys. Rev. Lett. **98**, 213904 (2007).
6. Y. F. Xiao, X. B. Zou, W. Jiang, Y. L. Chen, and G. C. Guo, Phys. Rev. A **75**, 063833 (2007).
7. T. W. Ebbesen, C. Genet, and S. I. Bozhevolnyi, Phys. Today **61**(5), 44 (2008).
8. D. K. Gramotnev and S. I. Bozhevolnyi, Nat. Photonics **4**, 83 (2010).
9. Y. Huang, C. Min, and G. Veronis, Appl. Phys. Lett. **99**, 143117 (2011).
10. L. Yang, C. G. Min, and G. Veronis, Opt. Lett. **35**, 4184 (2010).
11. Y. Zhang, S. Darmawan, L. Y. M. Tobing, T. Mei, and D. H. Zhang, J. Opt. Soc. Am. B **28**, 28 (2011).
12. Z. H. Han and S. I. Bozhevolnyi, Opt. Express **19**, 3251 (2011).
13. G. X. Wang, H. Lu, and X. M. Liu, Opt. Express **20**, 20902 (2012).
14. H. Lu, X. M. Liu, and D. Mao, Phys. Rev. A **85**, 053803 (2012).
15. H. Lu, X. M. Liu, D. Mao, Y. K. Gong, and G. X. Wang, Opt. Lett. **36**, 3233 (2011).
16. X. J. Piao, S. Yu, S. Koo, K. H. Lee, and N. Park, Opt. Express **19**, 10907 (2011).
17. Y. H. Guo, L. S. Yan, W. Pan, B. Luo, K. H. Wen, Z. Guo, and X. G. Luo, Opt. Express **20**, 24348 (2012).
18. R. D. Kekatpure, Phys. Rev. Lett. **104**, 243902 (2010).
19. H. A. Haus and W. P. Huang, Proc. IEEE **79**, 1505 (1991).
20. H. A. Haus, *Waves and Fields in Optoelectronics* (Prentice-Hall, 1984), Chap. 7.
21. G. T. Cao, H. J. Li, S. P. Zhan, H. Q. Xu, Z. M. Liu, Z. H. He, and Y. Wang, Opt. Express **21**, 9198 (2013).
22. L. Chen, C. M. Gao, J. M. Xu, X. F. Zang, B. Cai, and Y. M. Zhu, Opt. Lett. **38**, 1379 (2013).
23. A. Taflove and S. Hagness, *Computational Electrodynamics: The Finite-Difference Time-Domain Method*, 2nd ed. (Artech House, 2000).
24. E. D. Palik, *Handbook of Optical Constants in Solids* (Academic, 1982).
25. E. N. Economou, Phys. Rev. **182**, 539 (1969).
26. P. B. Johnson and R. W. Christy, Phys. Rev. B **6**, 4370 (1972).
27. A. Ishikawa, R. F. Oulton, T. Zentgra, and X. Zhang, Phys. Rev. B **85**, 155108 (2012).
28. G. X. Wang, H. Lu, and X. M. Liu, Opt. Lett. **38**, 558 (2013).
29. T. Zentgraf, S. Zhang, R. F. Oulton, and X. Zhang, Phys. Rev. B **80**, 195415 (2009).
30. K. Ooi, T. Okada, and K. Tanaka, Phys. Rev. B **84**, 115405 (2011).